

Modeling of Ni_4Ti_3 precipitation during stress-free and stress-assisted aging of bi-crystalline NiTi shape memory alloys

KE Chang-bo^{1,2}, CAO Shan-shan², MA Xiao², ZHANG Xin-ping²

1. School of Mechanical and Automotive Engineering, South China University of Technology, Guangzhou 510640, China;
2. School of Materials Science and Engineering, South China University of Technology, Guangzhou 510640, China

Received 9 July 2012; accepted 6 August 2012

Abstract: The phase field method was applied to study the microstructure evolution of Ni_4Ti_3 precipitates during stress-free and stress-assisted aging of bi-crystalline NiTi shape memory alloys (SAMs) with two different initial Ni-contents of 51.5% and 52.5% (mole fraction), respectively. The simulation results show that, during stress-free aging of the NiTi alloy with a low supersaturation of Ni (i.e., Ti–51.5%Ni), the Ni_4Ti_3 precipitates exhibit a heterogeneous distribution with a high number density of particles at the grain boundary, leaving most of the grain interiors free of precipitates; while for the NiTi alloy with a high supersaturation of Ni (i.e., Ti–52.5%Ni), the Ni_4Ti_3 precipitates show a homogeneous distribution across the entire simulation system. The stress-assisted aging can give rise to homogeneous distribution of the precipitates, regardless of the initial Ni-content; however, the distribution of variant type within the two grains is heterogeneous.

Key words: NiTi shape memory alloy; Ni_4Ti_3 precipitate; low-angle grain boundary; martensitic transformation; phase field simulation

1 Introduction

Near-equiatomic NiTi alloys have attracted a great deal of interests in the past decades on account of excellent shape memory effect and superelastic property. They have become one of the most important metal functional materials widely used in the field of aerospace and aeronautical engineering, as well as in biomedical engineering and technology. Generally, the NiTi shape memory alloys (SMAs) may undergo aging treatment leading to the metastable precipitation of Ni_4Ti_3 particles which possess the lenticular and disc-like morphologies in 2D and 3D observation [1], respectively. Experimental characterizations showed that the coherently distributed Ni_4Ti_3 particles have rhombohedral structure with space group $R\bar{3}$ and can form four groups of variants, in which each group takes different $(111)_{B_2}$ as the habit plane and owns a pair of conjugate variants [2,3]. Further, it has been well understood that the presence of Ni_4Ti_3 particles favors the formation of R-phase rather than B19' martensite since the latter produces larger lattice

deformation [4]. The study of the influence of Ni_4Ti_3 on martensitic transformation was mainly performed by experimental observation and characterization such as differential scanning calorimetry (DSC) and in situ transmission electron microscopy (TEM) [5–7]. Thus far, it has been well recognized that the martensitic transformation behavior in NiTi SMAs is associated with the distribution of Ni_4Ti_3 particles, while the distribution behavior of Ni_4Ti_3 precipitates can be affected by several factors including the heat treatment condition, initial Ni/Ti atomic ratio and the applied external stress. However, there is a serious lack of understanding of the comprehensive effect of the grain boundary in polycrystal (or bi-crystal for simplicity) and the initial supersaturation level of Ni-content as well as the external stress on the distribution of Ni_4Ti_3 precipitates. Moreover, it has been noticed that the previous simulation studies [8–10] were confined within single crystal or single precipitate variant, while polycrystalline and multiple precipitate variants are of great importance in practical applications and the corresponding simulation work is indeed imperative [11]. In addition, some simulation

inputs in the previous works [8–10] were not accurate due to the technique limitations in the original experimental study [12]. With the rapid development in experiments and simulation technology, nowadays the model inputs can be calculated precisely [13].

In order to clarify the above comprehensive effect and the heterogeneous precipitation of Ni₄Ti₃ particles, the present study employs more accurate model inputs and extends the phase field model [8–10] to simulate the precipitation behavior of Ni₄Ti₃ phase in bi-crystalline NiTi alloys and, the focus is placed on identifying the effect of different initial supersaturation levels of Ni-content, grain boundary and external stress on the microstructure evolution and distribution behavior of Ni₄Ti₃ precipitates.

2 Phase field model

In the phase field model, the bulk chemical free energy of all phases, the interfacial energy and the elastic strain are necessary inputs. The equilibrium shapes of all phases are determined by the competition and interaction of the above energies. These energies for Ni₄Ti₃ precipitation will be briefly introduced as follows.

2.1 Total chemical free energy

Assuming isotropic interface properties, the total chemical free energy, including the bulk free energy expressed by adopting a Landau polynomial and the interfacial energy characterized by gradient terms, can be written as [8]:

$$F_{\text{ch}} = \int d^3\mathbf{r} \left\{ f[C(\mathbf{r}), \eta_p(\mathbf{r})] + \frac{k_C}{2} [\nabla C(\mathbf{r})]^2 + \sum_{p=1}^v \frac{k_\eta}{2} [\nabla \eta_p(\mathbf{r})]^2 \right\} \quad (1)$$

where $C(\mathbf{r})$ and $\eta_p(\mathbf{r})$ are composition field and order parameter field, respectively; v is the number of Ni₄Ti₃ variant groups, here $v=4$; k_C and k_η are the gradient energy coefficients for composition and order parameter field, respectively.

2.2 Elastic energy

According to KHACHATURYAN's micro-elasticity theory [11], the modulus of Ni₄Ti₃ precipitate is supposed to be the same as that of the B2 matrix. The elastic constants used in this study are: $C_{11}=162$ GPa, $C_{12}=129$ GPa and $C_{44}=34$ GPa [12]. The elastic energy can be expressed by the following equation:

$$E_{\text{el}} = \frac{1}{2} \int \frac{d^3\mathbf{k}}{(2\pi)^3} [C_{ijkl} \tilde{\varepsilon}_{ij}^0(\mathbf{k}) \tilde{\varepsilon}_{kl}^0(\mathbf{k})]^* - \mathbf{n}_i \tilde{\sigma}_{ij}^0(\mathbf{k}) \mathbf{\Omega}_{jk}(\mathbf{n}) \sigma_{kl}^0(\mathbf{k})^* \mathbf{n}_l] - \int_V \sigma_{ij}^{\text{appl}} \varepsilon_{ij}^0(\mathbf{r}) d^3\mathbf{r} \quad (2)$$

where C_{ijkl} is the elastic constants, $\tilde{\varepsilon}_{ij}^0(\mathbf{k})$ is the Fourier

transform of the local stress-free transformation strain $\varepsilon_{ij}^0(\mathbf{r})$, \mathbf{n}_i is the unit vector in the reciprocal space, $\tilde{\sigma}_{ij}^0(\mathbf{k}) = C_{ijkl} \tilde{\varepsilon}_{kl}^0(\mathbf{k})$, $\mathbf{\Omega}_{jk}(\mathbf{n})$ is the inverse matrix of the Green function $\mathbf{\Omega}_{jk}^{-1}(\mathbf{n}) = C_{ijkl} e_i e_l$. The integral calculation must exclude a volume $(2\pi)^3/V$ in the reciprocal space at $\mathbf{g}=0$, and here V denotes the total volume of the system. $\sigma_{ij}^{\text{appl}}$ is the external stress, $\varepsilon_{ij}^0(\mathbf{r})$ is assumed to be linearly dependent on the square of the structural order parameter through stress-free transformation strain $\varepsilon_{ij}^0(p)$, the value of ε_{ij}^0 in its principal reference is chosen as [13,14]:

$$\varepsilon_{ij}^0 = \begin{bmatrix} -0.00417 & 0 & 0 \\ 0 & -0.00417 & 0 \\ 0 & 0 & -0.0257 \end{bmatrix} \quad (3)$$

2.3 Description of grain boundary energy

In this study, bi-crystal is considered to be a simple system which contains two grains with different orientations and a grain boundary between them. We consider the segregation effect when describing the grain boundary. The phase field grain boundary segregation model similar to those of KIM and PARK [15] and GRONHAGEN and ARGENT [16] was used. Another phase field $\phi_i (i=1, 2)$ is assigned to depict the two grains. The values of ϕ_i in the grain boundary region change gradually from $\phi_1=1$ ($\phi_2=0$) to $\phi_1=0$ ($\phi_2=1$). Since the grain boundary is immobile in the model, in which only one column is assigned, the values of ϕ_i can be manually set as $\phi_1=\phi_2=0.5$. Taking grain boundary into account, the total free energy can be rewritten as:

$$F_{\text{ch}} = \int_V [f(C(\mathbf{r}), \eta_p(\mathbf{r})) + \frac{k_C}{2} (\nabla C(\mathbf{r}))^2 + \sum_{p=1}^v \frac{k_\eta}{2} (\nabla \eta_p(\mathbf{r}))^2 + \frac{\varepsilon}{2} \sum_{i=1}^2 |\nabla \phi_i|^2 + W(C(\mathbf{r})) \sum_{i=1}^2 g(\phi_i)] d^3\mathbf{r} \quad (4)$$

where ε is the gradient energy coefficient, the function of $g(\phi)$ is a double-well potential which satisfies $g(0)=g(1)=1$, and $W(C(\mathbf{r}))$ stands for the height of the potential. The last two terms in Eq. (4) are the energy contributions from the grain boundary. In the present study, $g(\phi_i) = \phi_i^2(1-\phi_i)^2$ is introduced to characterize the double-well potential. Considering the grain boundary segregation, $W(C(\mathbf{r}))$ should decrease with the solute (Ni) concentration, while in this study the $W(C(\mathbf{r}))$ increases with increasing $C(\mathbf{r})$ which denotes Ti concentration. Moreover, once Ni₄Ti₃ precipitates form at the grain boundary, the value of $W(C(\mathbf{r}))$ is minimized due to the replacement of the grain boundary by Ni₄Ti₃ particles; thus, the function of $W(C(\mathbf{r}))$ can be expressed by:

$$W(C(\mathbf{r})) = (1 + \chi C(\mathbf{r})) \varpi \cdot (1 - b \sum_{p=1}^v \eta_p^2) \quad (5)$$

where χ is a parameter relating the interactions between the solute atoms and the grain boundary, ϖ is the grain boundary energy density.

2.4 Kinetic equations for microstructure evolution

The microstructure evolution is determined by the following equations:

$$\frac{\partial \eta_p(\mathbf{r}, t)}{\partial t} = -L_\eta \frac{\delta F}{\delta \eta_p(\mathbf{r}, t)} + \xi_\eta(\mathbf{r}, t) \quad (6)$$

$$\frac{\partial C(\mathbf{r}, t)}{\partial t} = \nabla \cdot \{M_C \nabla \frac{\delta F}{\delta C(\mathbf{r}, t)}\} + \xi_C(\mathbf{r}, t) \quad (7)$$

where L_η and M_C are the mobility of the order parameter and chemical mobility, respectively. Two sets of order parameters are needed to define the bi-crystal, and each set includes four order parameters corresponding to the four Ni_4Ti_3 variants whose habit planes belong to different $\{111\}_{\text{B2}}$. To facilitate the computation, Eqs. (6) and (7) should be converted into dimensionless forms. $G_0=C_{44}=34 \text{ GPa}=34 \times 10^9 \text{ J/m}^3$, $M_0=1.008 \times 10^{-26} \text{ mol}^2/(\text{J}\cdot\text{m}\cdot\text{s})$ [17,18] are chosen as the normalized factors for energy and mobility, respectively. The dimensionless numerical values of gradient coefficients are set as $k_\eta^*=1.0$ and $k_C^*=0.01$. In order to keep computational stability, the dimensionless values of kinetic coefficients are assigned as $L^*=3.0$ and $M^*=1.0$. Due to the lack of accurate parameter values in Eq. (5), all the values are chosen from a previous study [15], i.e., $\chi=4$, $\varpi=2$, $\xi=0.1$ and $b=1$.

3 Simulation results and discussion

In our simulation, small angle grain boundary was taken into account due to the limitation of the submodels in Refs. [15,16]. The misfit angle was set as $\theta=10^\circ$, which means the right-hand grain is rotated by 10° along $[001]_{\text{B2}}$ from the left-hand grain, in which the frame is the same as the B2 frame, i.e., the simulation coordinate.

In the simulation, a computation cell of $512l_0 \times 512l_0 \times 1l_0$ was employed. The initial values of all order parameters were set to zero; different initial values of $C(\mathbf{r}, t)$ were set as 0.43 and 0.42, which are corresponding to the Ni atom fraction dropping into 0.515 and 0.525, respectively. In the initial 1500 time steps, the two noise terms in Eq. (6) were switched on to imitate the random nucleation. In order to investigate the effect of the external stress on the precipitate microstructure, different levels of uniaxial compressive stresses, whose non-zero component was set as $\sigma^*=-0.0025$ (85 MPa) and $\sigma^*=-0.005$ (170 MPa) respectively, were initially applied to the system, and this effect is similar to the experimental study of stress-assisted aging of the NiTi matrix [5,6].

3.1 Ni_4Ti_3 precipitate microstructure during stress-free aging of bi-crystalline NiTi alloys with different initial supersaturation levels of Ni-content

To better present the simulation results, the Ni_4Ti_3 precipitate variants with different crystallographic orientations are classified into four $\{111\}_{\text{B2}}$ types, as shown in Table 1.

Table 1 Classification of Ni_4Ti_3 variants and variant scheme in simulation coordinate

Variant type	Variant plane normal	Variant scheme in simulation frame
1	$\pm[111]_{\text{B2}}$	
2	$\pm[\bar{1}11]_{\text{B2}}$	
3	$\pm[\bar{1}\bar{1}1]_{\text{B2}}$	
4	$\pm[11\bar{1}]_{\text{B2}}$	

Figure 1 shows the microstructure evolution of Ni_4Ti_3 precipitates in the NiTi alloy with the initial Ni-content of 51.5% (mole fraction). Clearly, the Ni_4Ti_3 precipitates prefer to nucleate at the grain boundary region and a sharp portion of the precipitates dominate at and near the grain boundary; while in the grain interior, less precipitates can nucleate and grow. It is also noticed that the precipitates at the grain boundary show a smaller size than those in the grain interior, and the small size particles can be attributed to the simultaneous nucleation and competitive growth at the grain boundary; whereas, in the grain interior, the randomly nucleated precipitates can grow without any retardation. The heterogeneous distribution of Ni_4Ti_3 precipitates obtained in the present simulation is in good agreement with the previous results acquired by TEM observations [5–7], in which the grain boundary is enriched in smaller size Ni_4Ti_3 precipitates, while the grain interiors are sparsely occupied by larger size Ni_4Ti_3 particles, as typically shown in Fig. 1(d). Thus, it can be generally concluded that the grain boundary plays an important role in bringing the heterogeneous distribution of Ni_4Ti_3 precipitates during aging of the NiTi matrix with a low level of initial supersaturation of Ni-content.

In contrast to the above heterogeneous distribution, however, Ni_4Ti_3 particles precipitate uniformly when the initial Ni-content is 52.5% (mole fraction), as shown in Fig. 2. The nucleation of Ni_4Ti_3 particles seems homogeneous throughout the simulation system, a great number of precipitates fairly uniformly distribute across

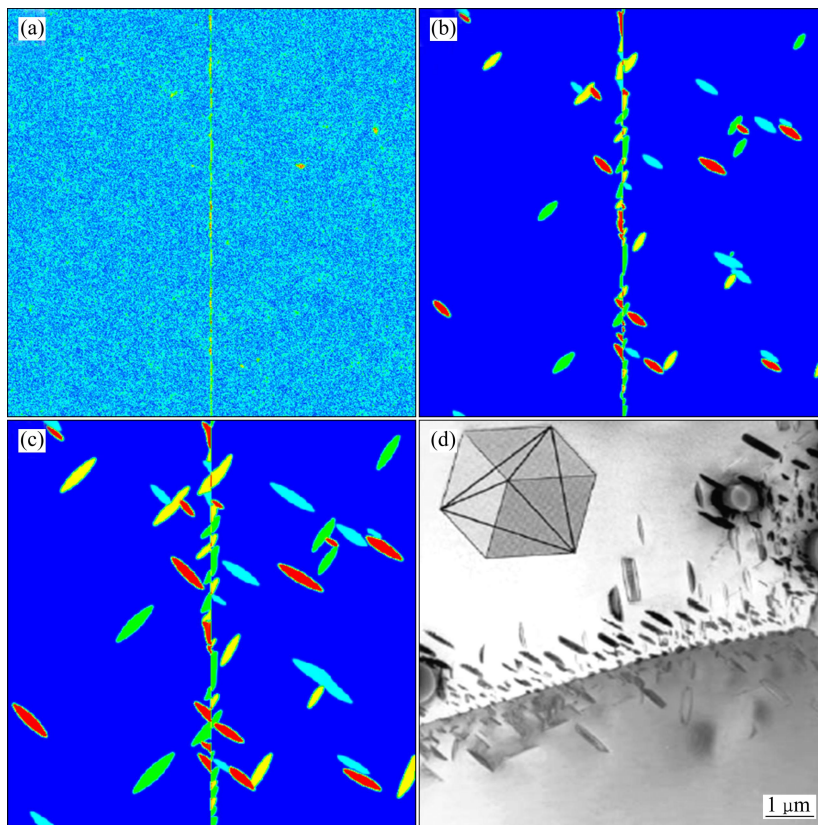


Fig. 1 Phase field simulation of Ni_4Ti_3 precipitation during stress-free aging of Ti–51.5%Ni bi-crystalline NiTi alloy: (a) $t^*=1500$; (b) $t^*=2500$; (c) $t^*=5000$; (d) TEM micrograph of Ni_4Ti_3 precipitates in NiTi alloy (with a nominal composition of 50.7%Ni) subjected to stress-free aging [5] (Photograph courtesy of Prof. Gunther Eggeler, Ruhr-University Bochum, Germany)

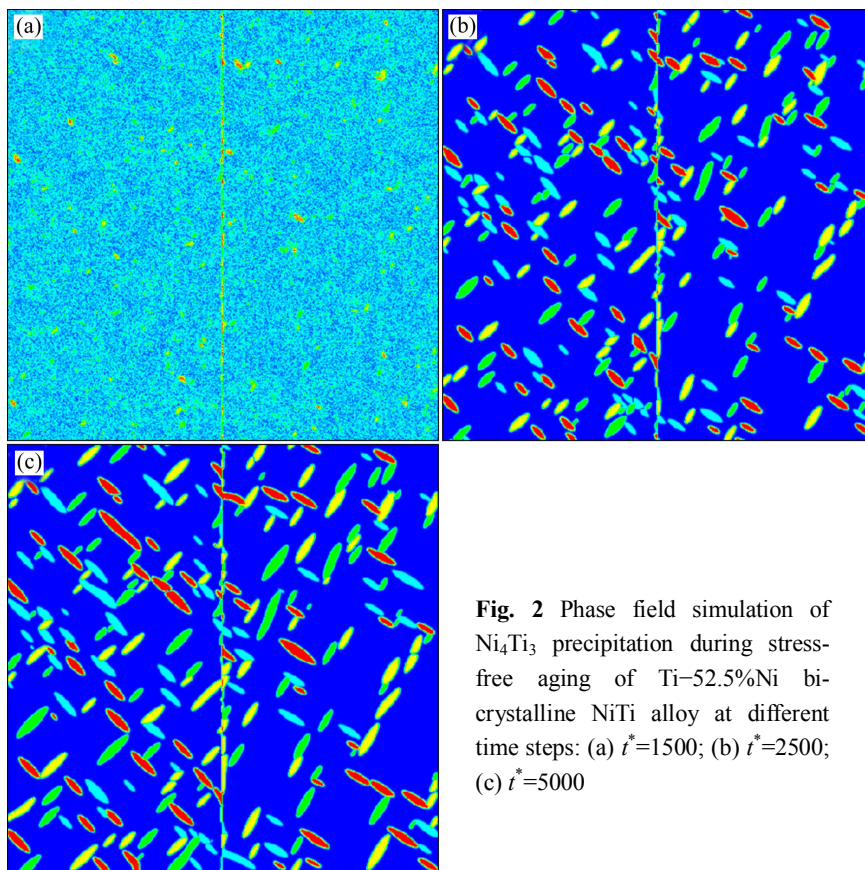


Fig. 2 Phase field simulation of Ni_4Ti_3 precipitation during stress-free aging of Ti–52.5%Ni bi-crystalline NiTi alloy at different time steps: (a) $t^*=1500$; (b) $t^*=2500$; (c) $t^*=5000$

the system and the grain boundary preference is not drastically apparent compared to the one with a low Ni-content of 51.5%. This means that the high supersaturation of Ni-content can generate a high driving force in the entire system in which the effect of the grain boundary energy may be suppressed to a certain extent. Further, the results may imply that whether the distribution of Ni_4Ti_3 precipitates in bi-crystal or polycrystal is homogenous or heterogeneous depends not only on the grain boundary energy but also on the initial supersaturation level of Ni-content in the NiTi alloy, and the competition between these two factors determines the precipitation behavior during stress-free aging of the NiTi alloy.

Figure 3 shows the statistical results of the area fraction distribution of Ni_4Ti_3 precipitates across the entire bicrystal system. In the statistical analysis, the whole simulation system was divided into 25 continuous sections, and each section covered an area of 20 (along $[100]_{\text{B2}} \times 512$ (along $[010]_{\text{B2}}$) grid points except the center region which occupied an area of 32×512 grid points. The total grid points (GP_T) occupied by the

precipitates were counted by the computer, and the area fraction of the precipitates was calculated by GP_T/A (here, A means the specific section area). Figure 3(a) clearly shows that the area fraction near the grain boundary is obviously larger than that in the grain interior, meaning that the Ni_4Ti_3 particles tend to precipitate near the grain boundaries. However, the distribution feature of the precipitates for the alloy with a higher Ni-content (i.e., 52.5%) changes, as shown in Fig. 3(b), where the grain boundary region shows no distinct peak value of the distribution and there is nearly no big difference in the area fraction among all sections. This can well support the conclusion that the homogeneous nucleation of Ni_4Ti_3 particles may easily occur in the NiTi alloy matrix with a high supersaturation level of Ni.

The above results may be helpful for the prediction of the subsequent martensitic transformation behavior. Based on the simulation results, it is reasonable to see that the stress-free aging of the NiTi matrix with a low supersaturation level of Ni can induce B2-R-B19' transformation preferentially at the grain boundary area where Ni_4Ti_3 precipitates concentrate, while B2-B19' transformation may occur dominantly in the grain interior where the most part is precipitate free. However, the aging process of NiTi bicrystalline matrix with a high supersaturation level of Ni may lead to the homogeneous nucleation of R-phase across the whole matrix without the preferential nucleation of R-phase in the grain boundary region. It should be pointed out that although the present work is incapable of predicting the martensitic transformation sequence in the matrix, the prediction based on the current simulation is consistent with some previous experimental results [6,7].

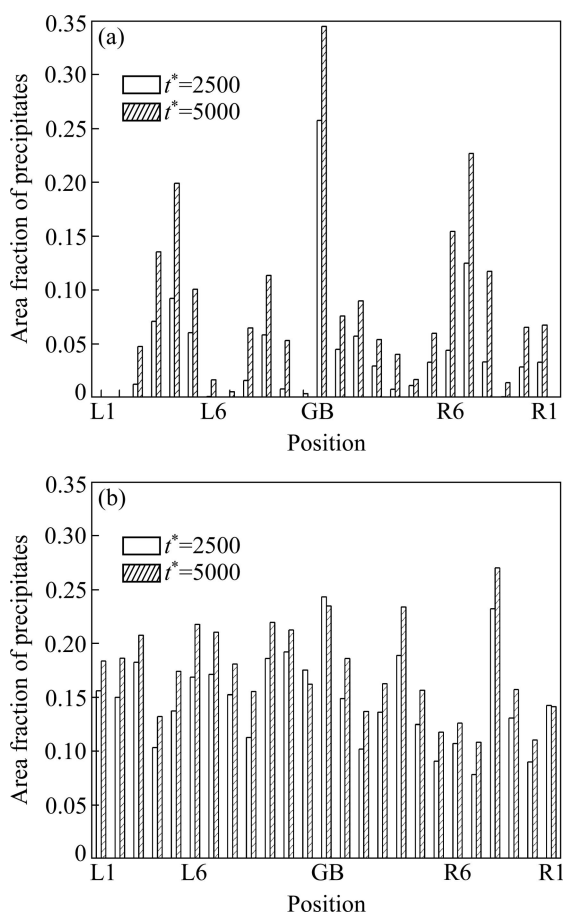


Fig. 3 Area fraction distribution of Ni_4Ti_3 particles across entire matrix during stress-free aging of NiTi alloys: (a) Ti-51.5%Ni; (b) Ti-52.5%Ni ($Lx(x=1, 2, \dots, 12)$ and $Rx(x=1, 2, \dots, 12)$ represent divided sections in left-hand and right-hand grains, respectively)

3.2 Ni_4Ti_3 precipitates microstructure during stress-assisted aging of bi-crystalline NiTi alloys with different initial supersaturation levels of Ni-content

Phase field simulation results of the precipitation of Ni_4Ti_3 particles in NiTi alloys under different levels of compressive stress are shown in Fig. 4. For the Ti-51.5%Ni alloy after aging under the compressive stress of 85 MPa and 170 MPa along $[100]_{\text{B2}}$, it is clear that the heterogeneous particle distribution caused by the grain boundary segregation disappears; instead, the distribution of Ni_4Ti_3 precipitates is homogeneous in the number density in the whole system, regardless of stress levels, as shown in Figs. 4(a) and (b). The similar precipitation behavior and microstructure evolution can be seen in the NiTi alloy with a higher initial Ni-content (i.e., 52.5%), as shown in Figs. 4(c) and (d). This means that the existence of the applied stress can weaken the grain boundary effect, while promoting the homogeneous nucleation. Thus, the homogeneous distribution in the

number density becomes the dominant feature. Figure 5 shows the area fraction distributions in these cases, which clearly presents the homogeneous precipitation behavior in the NiTi matrix during stress-assisted aging. For the NiTi matrix with a lower supersaturation level of Ni-content (i.e., 51.5%), the area fraction near the grain boundary is slightly higher than that at other places, but no obvious difference is observed compared to the case undergoing stress-free aging as shown in Fig. 3(a).

In addition, it can also be seen clearly in Fig. 4 that

the number density of each type of variant in the right-hand grain is different from that in the left-hand grain, regardless of the initial Ni-content and the selected stress. In the left-hand grain, the four types of variants are almost equal in the area fraction, while type 2 and 3 variants exist dominantly in the right-hand grain, as shown in Table 2. This phenomenon was reported as a kind of heterogeneity [19], while the present simulation results suggest that this behavior is more likely to be attributed to the external stress which brings about

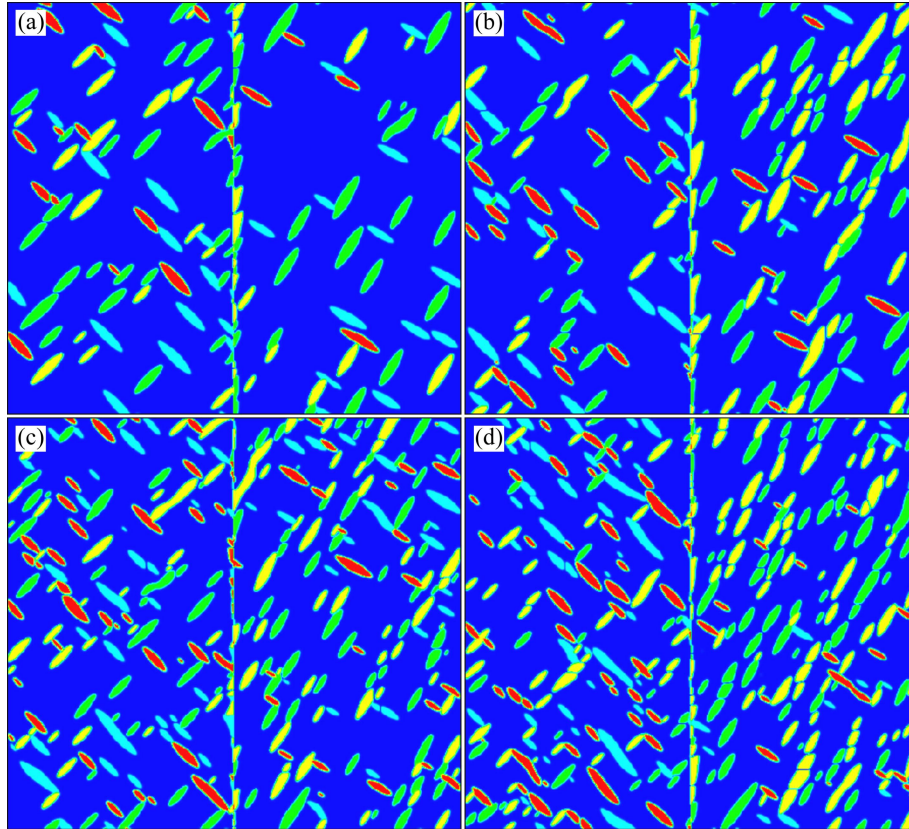


Fig. 4 Phase field simulation of microstructure evolution of Ni_4Ti_3 precipitates in bi-crystalline NiTi alloys under different compressive stresses at $t^*=5000$: (a) Ti-51.5%Ni, $\sigma=-85$ MPa; (b) Ti-51.5%Ni, $\sigma=-170$ MPa; (c) Ti-52.5%Ni, $\sigma=-85$ MPa; (d) Ti-52.5%Ni, $\sigma=-170$ MPa

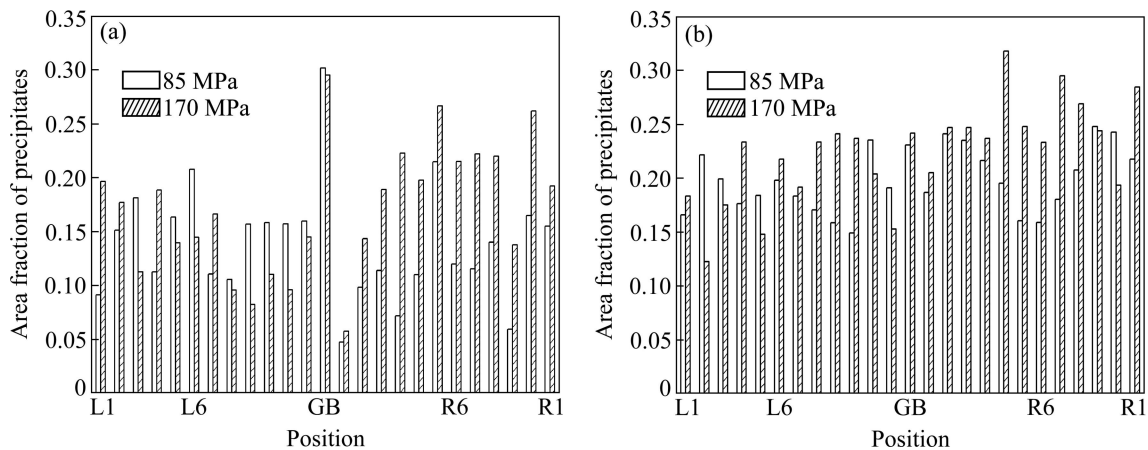


Fig. 5 Area fraction distribution of Ni_4Ti_3 particles across entire matrix during stress-assisted aging of NiTi alloys with two different initial supersaturation levels of Ni-content: (a) Ti-51.5%Ni; (b) Ti-52.5%Ni

Table 2 Statistical results of area fraction of Ni₄Ti₃ precipitate variants in each grain (%)

Simulation condition		Variant type			
Ni-content, stress	Left or right grain	1	2	3	4
0.515% Ni, 85 MPa	L	3.43	3.78	4.19	3.56
	R	3.75	5.19	4.94	0.67
0.515% Ni, 170 MPa	L	4.87	2.84	2.72	3.55
	R	2.89	6.68	7.75	1.39
0.525% Ni, 85 MPa	L	4.25	4.57	3.58	4.09
	R	2.70	6.04	6.05	2.17
0.525% Ni, 170 MPa	L	5.29	5.48	5.73	5.69
	R	3.88	8.93	8.28	1.19

selective nucleation and growth of Ni₄Ti₃ particles through the adjacent misorientational grains. Moreover, the degree of this kind of inhomogeneity becomes slightly distinct under a higher stress.

From the above simulation results, it is indicated that the grain boundary effect is dependent on the composition (or supersaturation) and stress. In the NiTi alloy with a low supersaturation level of Ni-content (i.e., 51.5%), the Ni-rich grain boundary may favor the nucleation of precipitates, while for the one with high initial Ni-content (i.e., 52.5%), the Ni concentration difference between the grain boundary and grain interior is small, thus the precipitates generate homogeneously without obvious preference for precipitation in the grain boundary. Furthermore, the external stress can change the precipitation behavior of Ni₄Ti₃ particles and this effect can become more sensitive in the NiTi alloy with a low initial Ni-content compared to the one with a high Ni-content.

It is noticed that in the NiTi matrix with a high initial supersaturation level of Ni-content, the particle distribution seems to be independent of the existence of the external stress and its level; this demonstrates that the nucleation behavior not only depends on the applied external stress, but also on the initial concentration. However, the heterogeneous distribution behavior of the four types of precipitate variants across the two adjacent NiTi matrix grains may be mainly determined by the external stress. This distribution behavior was considered a kind of heterogeneity first introduced in Ref. [19].

Furthermore, it should also be pointed out that the stress in the present study indeed reaches a certain level. Through several times of simulation with different levels of stress, it is found that the particle distribution exhibits homogeneity in the entire bicrystal system when the stress reaches 65 MPa, in contrast to the slightly lower external stress of around 50 MPa in the previous experimental study [19]. However, the present study is incapable of providing the critical value of the external

stress, since there is lack of accurate free energies of both NiTi and Ni₄Ti₃ phases as well as the precise grain boundary parameters.

Due to the limitations of the submodels in Refs. [15,16], in which the description of grain boundary in terms of the order parameter in phase field model is confined to low-angle grain boundary, thus, the current work can only address the precipitation issue in bi-crystal with low-angle grain boundary, despite the model in present work is capable of simulating general high angle grain boundary. In future work, a more applicable model, including all angle levels of grain boundary will be employed to study the Ni₄Ti₃ precipitation in polycrystalline NiTi shape memory alloys.

4 Conclusions

1) In bi-crystalline NiTi alloys, the grain boundary plays a necessary but insufficient role in the heterogeneous distribution of Ni₄Ti₃ precipitates, in which the Ni₄Ti₃ particles prefer to precipitate in the grain boundary area and leave the most of the grain interiors free of precipitates, whereas the grain boundary effect is dependent on the composition of the alloy and the applied stress.

2) The applied compressive stress and the initial supersaturation level of Ni-content can suppress the grain boundary effect and consequently change the precipitation behavior of Ni₄Ti₃ particles. The effect of the external stress is more sensitive in the NiTi alloy with a low supersaturation level of Ni-content.

3) The initial supersaturation level of Ni-content seems to be the determinative factor in the number density of Ni₄Ti₃ precipitates, while the heterogeneous distribution of each type of variant across the two adjacent grains with different orientations is mainly controlled by the external stress.

References

- [1] SABURI T, NENNO S, FUKUDA T. Crystal structure and morphology of the metastable X-phase in shape memory Ti–Ni alloy [J]. *Journal of Less Common Metals*, 1986, 125: 157–166.
- [2] NISHIDA M, WAYMAN C M, HONMA T. Precipitation processes in near equiatomic TiNi shape memory alloys [J]. *Metallurgical and Materials Transaction A*, 1986, 17: 1505–1515.
- [3] TADAKI T, NAKATA Y, SHIMIZU K, OTSUKA K. Crystal structure, composition and morphology of a precipitate in an aged Ti-50at%Ni shape memory alloy [J]. *Transaction of Japan Institute of Metals*, 1986, 27: 731–740.
- [4] REN X, MIURA N, ZHANG J, OTSUKA K, TANAKA K, KOIWA M, SUZUKI T, CHUMLYAKOV Y I, ASAI M. A comparative study of elastic constants of Ti–Ni-based alloys prior to martensitic transformation [J]. *Materials Science and Engineering A*, 2001, 312: 196–206.

- [5] ALLAFI J K, DLOUHY A, EGGELER G. Ni₄Ti₃-precipitation during aging of NiTi shape memory alloys and its influence on martensitic phase transformations [J]. Acta Materialia, 2002, 50: 4255–4274.
- [6] MICHUTTA J, SOMSEN C, YAWNY A, DLOUHY A, EGGELER G. Elementary martensitic transformation processes in Ni-rich NiTi single crystals with Ni₄Ti₃ precipitates [J]. Acta Materialia, 2006, 54: 3525–3542.
- [7] FAN G, CHEN W, YANG S, ZHU J H, REN X B, OTSUKA K. Origin of abnormal multi-stage martensitic transformation behavior in aged Ni-rich Ti–Ni shape memory alloys [J]. Acta Materialia, 2004, 52: 4351–4362.
- [8] LI D Y, CHEN L Q. Morphological evolution of coherent multi-variant Ti₁₁Ni₁₄ precipitates in Ti–Ni alloys under an applied stress—A computer simulation study [J]. Acta Materialia, 1998, 46: 639–649.
- [9] LI D Y. Morphological evolution of coherent Ti₁₁Ni₁₄ precipitates under inhomogeneous stresses [J]. Philosophical Magazine A, 1999, 79: 2603–2616.
- [10] MA XQ, SHI S Q, WOO C H, CHEN L Q. Simulation of γ -hydride precipitation in bi-crystalline zirconium under uniformly applied load [J]. Materials Science and Engineering A, 2002, 334: 6–10.
- [11] KHACHATURYAN A G. Theory of structural transformation in solids [M]. New York: Wiley-Interscience Publication, 1983: 213–214.
- [12] MERCIER O, MELTON K N, GREMAUD G, HAGI J. Single-crystal elastic constants of the equiatomic NiTi alloys near the martensitic transformation [J]. Journal of Applied Physics, 1980, 51: 1833–1834.
- [13] ZHOU N, SHEN C, WAGNER M F, EGGELER G, MILLS M J, WANG Y. Effect of Ni₄Ti₃ precipitation on martensitic transformation in Ti–Ni [J]. Acta Materialia, 2010, 58: 6685–6694.
- [14] KE Chang-bo, MA Xiao, ZHANG Xin-ping. Phase field simulation of the effect of applied external stress on growth kinetics of coherent Ni₄Ti₃ precipitate in NiTi alloy [J]. Acta Metallurgica Sinica, 2010, 46: 921–929. (in Chinese)
- [15] KIM S G, PARK Y B. Grain boundary segregation, solute drag and abnormal grain growth [J]. Acta Materialia, 2008, 56: 3739–3753.
- [16] GRONHAGEN K, AGREN J. Grain-boundary segregation and dynamic solute drag theory—A phase field approach [J]. Acta Materialia, 2007, 55: 955–960.
- [17] SHARMA S K, MACHT M P, NAUNDORF V. Impurity-diffusion investigations in amorphous Ti₆₀Ni₄₀ [J]. Physical Review B, 1994, 49: 6655–6666.
- [18] KE Chang-bo, MA Xiao, ZHANG Xin-ping. Phase field simulation of growth kinetics of coherent Ni₄Ti₃ precipitates in NiTi shape memory alloy [J]. Acta Metallurgica Sinica, 2010, 46: 84–90. (in Chinese)
- [19] BOJDA O, EGGELER G, DLOUHY A. Precipitation of Ni₄Ti₃-variants in a polycrystalline Ni-rich NiTi shape memory alloy [J]. Scripta Materialia, 2005, 53: 99–104.

双晶体 NiTi 形状记忆合金在无/有应力作用时效下的 Ni₄Ti₃ 相沉淀行为模拟

柯常波^{1,2}, 曹姗姗², 马 骁², 张新平²

1. 华南理工大学 机械与汽车工程学院, 广州 510640;
2. 华南理工大学 材料科学与工程学院, 广州 510640

摘 要: 运用相场方法研究双晶体 NiTi 形状记忆合金分别在无应力和有应力作用下时效过程中 Ni₄Ti₃ 相的沉淀行为, 模拟研究两种不同初始过饱和度(Ni 含量分别为 51.5%和 52.5%, 摩尔分数)的 NiTi 基体并考虑外加应力的影响。模拟结果表明, 在无应力作用的体系中, 当体系 Ni 原子初始浓度相对较低(51.5% Ni)时, Ni₄Ti₃ 相以非均匀的方式析出, 其中晶界上存在大量的 Ni₄Ti₃ 变体, 晶界内大部分区域无变体; 当体系 Ni 原子初始浓度较高(52.5% Ni)时, Ni₄Ti₃ 在整个双晶体系中均匀析出。在所研究的两种初始浓度下, 一定大小的外加应力将直接导致 Ni₄Ti₃ 变体在整个模拟体系中均匀析出, 而两晶粒中变体的类型分布有所不同。

关键词: NiTi 形状记忆合金; Ni₄Ti₃ 沉淀相; 小角度晶界; 马氏体相变; 相场法

(Edited by YUAN Sai-qian)